

# Plasma Double Layers at the Boundary between Venus and the Solar Wind

D.M. Malaspina<sup>1,2</sup>, K. Goodrich<sup>3</sup>, R. Livi<sup>3</sup>, J. Halekas<sup>4</sup>, M. McManus<sup>3</sup>, S.  
Curry<sup>3</sup>, S.D. Bale<sup>3,5</sup>, J.W. Bonnell<sup>3</sup>, T. Dudok de Wit<sup>6</sup>, K. Goetz<sup>7</sup>, P.R.  
Harvey<sup>3</sup>, R.J. MacDowall<sup>8</sup>, M. Pulupa<sup>3</sup>, A.W. Case<sup>9</sup>, J.C. Kasper<sup>10</sup>, K.E.  
Korreck<sup>9</sup>, D. Larson<sup>3</sup>, M.L. Stevens<sup>9</sup>, P. Whittlesey<sup>3</sup>

<sup>1</sup>Department of Astrophysical and Planetary Sciences, University of Colorado, Boulder, CO, USA

<sup>2</sup>Laboratory for Atmospheric and Space Physics, University of Colorado, Boulder, CO, USA

<sup>3</sup>Space Sciences Laboratory, University of California Berkeley, Berkeley, CA, USA

<sup>4</sup>University of Iowa, Iowa City, IA, USA

<sup>5</sup>Physics Department, University of California, Berkeley, CA, USA

<sup>6</sup>LPC2E, CNRS, and University of Orléans, Orléans, France

<sup>7</sup>School of Physics and Astronomy, University of Minnesota, Minneapolis, MN, USA

<sup>8</sup>NASA Goddard Space Flight Center, Greenbelt, MD, USA

<sup>9</sup>Harvard-Smithsonian Center for Astrophysics, Cambridge, MA, USA

<sup>10</sup>University of Michigan, Ann Arbor, MI, USA

## Key Points:

- Plasma double layers are detected near the Venusian bow shock
- Multiple double layers are identified in a small amount of burst data
- Kinetic processes may help mediate interaction between the solar wind and induced magnetospheres

This is the author manuscript accepted for publication and has undergone full peer review but has not been through the copyediting, typesetting, pagination and proofreading process, which

may lead to differences between this version and the Version of Record. Please cite this article

as doi: [10.1029/2020GL090115](https://doi.org/10.1029/2020GL090115)

## Abstract

The solar wind is slowed, deflected, and heated as it encounters Venus's induced magnetosphere. The importance of kinetic plasma processes to these interactions has not been examined in detail, due to a lack of constraining observations. In this study, kinetic-scale electric field structures are identified in the Venusian magnetosheath, including plasma double layers. The double layers may be driven by currents or mixing of inhomogeneous plasmas near the edge of the magnetosheath. Estimated double layer spatial scales are consistent with those reported at Earth. Estimated potential drops are similar to electron temperature gradients across the bow shock. Many double layers are found in few high cadence data captures, suggesting that their amplitudes are high relative to other magnetosheath plasma waves. These are the first direct observations of plasma double layers beyond near-Earth space, supporting the idea that kinetic plasma processes are active in many space plasma environments.

## Plain Language Summary

Venus has no internally generated magnetic field, yet electric currents running through its ionized upper atmosphere create magnetic fields that push back against the flow of the solar wind. These induced fields cause the solar wind to slow and heat as the flow is deflected around Venus. This work reports observations of very small plasma structures that accelerate particles, identifiable by their characteristic electric field signatures, at the boundary where the solar wind starts to be deflected. The small plasma structures observed at Venus have been studied in near-Earth space for decades, but have never before been found near another planet. These structures are known to be important to the physics of strong electrical currents in space plasmas and the blending of dissimilar plasmas. Their identification at Venus is a strong demonstration that these small plasma structures are a universal plasma phenomena, at work in many plasma environments.

## 1 Introduction

Venus does not have an intrinsic magnetic field. It does have a thick neutral atmosphere that is ionized by solar photons, forming a conducting ionosphere that supports currents. The time-variable interplanetary magnetic field (IMF),  $B_{\text{IMF}}$ , drives currents in the ionosphere, which induce magnetic fields to oppose those in the IMF. These induced fields produce a magnetic obstacle to the solar wind, against which the IMF magnetic field 'piles up' and drapes (Futaana et al., 2017) and references therein).

Venus's induced magnetosphere exhibits structures analogous to those found where the solar wind encounters magnetized planets, including a bow shock, magnetosheath, and magnetotail. These structures have significantly different character at Venus than at Earth. At Venus, the upstream bow shock stand off distance is less than one planetary radius from the surface (e.g. (Martinez et al., 2009)). At Earth, it is  $\sim 12$  Earth radii. Knudsen et al. (2016) found that, at Venus, transformation of a significant portion of incident solar wind kinetic energy into ion and electron thermal energy was localized to a thin (100 - 200 km) layer, co-located with observations of non-Maxwellian electron distributions and the bow shock magnetic ramp. Pressure from heated sheath electrons, combined with the convective electric field, are important for defining the altitude of the ion composition boundary which separates the solar wind from the planetary plasma (Martinez et al., 2008).

Both ion and electron foreshocks, due to solar wind particles reflecting at the Venus bow shock, have been identified, and limited exploration of the waves associated with those structures was made using a 4-frequency spectrum analyzer on Pioneer Venus Orbiter (Russell et al., 2006) (active 1978-1992). However, identification of specific wave



70 modes was difficult, and few spacecraft with electric field instruments have visited Venus  
71 since, all with brief encounters (Futaana et al., 2017). Therefore, the role of kinetic wave-  
72 particle interactions in mediating the interaction between the solar wind and Venus's in-  
73 duced magnetosphere has not been comprehensively addressed by observations.

74 Parker Solar Probe (PSP) uses seven gravitational encounters with Venus to lower  
75 its solar orbital periapsis (Fox et al., 2016). The encounters require PSP to pass close  
76 to Venus ( $< 1$  Venus radii altitude), resulting in passage through its induced magneto-  
77 sphere. At the time of writing, PSP has returned data from three Venus encounters. This  
78 work focuses on the second encounter, which occurred on 26 December, 2019.

79 Several PSP instruments were powered on during the Venus encounters, including  
80 FIELDS (Bale et al., 2016). The PSP Venus encounters are the first time that an elec-  
81 tric field instrument has visited near-Venus space (Futaana et al., 2017) since two brief  
82 encounters with Venus by the Cassini spacecraft in 1998 and 1999 (Gurnett et al., 2001)  
83 and the first DC-coupled electric field instrument near Venus since Vega in 1985 (Klimov  
84 et al., 1986).

85 The FIELDS burst data enable relatively long captures of high cadence time se-  
86 ries fields data. In near Earth space, such data enabled observations of kinetic-scale elec-  
87 tric field structures, such as electron phase space holes and plasma double layers (e.g.  
88 (Matsumoto et al., 1994; Franz et al., 1998; Ergun et al., 2001; Cattell et al., 2002; J. S. Pick-  
89 ett et al., 2003; Ergun et al., 2009; S. Li et al., 2015; Mozer et al., 2013; Malaspina et  
90 al., 2014; Holmes, Ergun, Newman, Ahmadi, et al., 2018; Fu et al., 2020)). These struc-  
91 tures characteristically feature strong electric fields parallel to the background magnetic  
92 field, and they appear in kinetically unstable plasmas (e.g. (Schamel, 2012; Hutchinson,  
93 2017) and references therein), often in association with magnetic-field aligned currents  
94 (Ergun et al., 2001; Mozer et al., 2014) or near the interface between two disparate plasma  
95 populations as they homogenize (J. Pickett et al., 2004; Malaspina et al., 2014; Holmes,  
96 Ergun, Newman, Wilder, et al., 2018). In near-Earth space, kinetic-scale electric field  
97 structures have been identified in virtually every region where significant wave-particle  
98 energy transfer occurs and instrumentation capable of observing them is present, includ-  
99 ing the auroral region (Ergun et al., 2001), plasma sheet (Matsumoto et al., 1994; Er-  
100 gun et al., 2009), radiation belts (Mozer et al., 2013; Malaspina et al., 2014), magnetosheath  
101 (Cattell et al., 2002; J. S. Pickett et al., 2003), and bow shock (S. Li et al., 2015; Goodrich  
102 et al., 2018).

103 While kinetic-scale electric field structures have been identified and studied exten-  
104 sively at Earth, they have not been reported at induced magnetospheres such as Venus  
105 or Mars. Double layers in particular have not been reported in any planetary magne-  
106 tosphere except Earth's. Considering the ubiquity of kinetic-scale electric field structures  
107 in the Earth's magnetosphere, and their prominent role in the kinetic physics of mag-  
108 netic field-aligned currents and plasma homogenization, these structures are very likely  
109 to be present in induced planetary magnetospheres, but have remained undetected due  
110 to the small number of observations capable of detecting them.

111 In this work, observations of electron phase space holes and plasma double layers  
112 at the interface between Venus and the solar wind are reported, and their significance  
113 for the near-Venus plasma environment is discussed.

## 114 **2 Data and Processing**

115 This study makes use of data from the FIELDS (Bale et al., 2016) and SWEAP  
116 (Kasper et al., 2016) instrument suites on the PSP spacecraft.

117 FIELDS measures electric and magnetic fields across a broad frequency range: DC  
118 - 20 MHz for electric fields, and DC - 1 MHz for magnetic fields. The electric field sen-

119 sors consist of four  $\sim 2$  m antennas in the plane of the heat shield ( $V_1, V_2, V_3, V_4$ ) and  
 120 one  $\sim 21$  cm antenna mounted on the magnetometer boom 'tail' of the spacecraft ( $V_5$ ).  
 121 The magnetic field sensors include two fluxgate magnetometers (FGM) and one search  
 122 coil magnetometer (SCM) mounted to the magnetometer boom.

123 The low-energy particle instrument suite, SWEAP, consists of four detectors: the  
 124 Solar Probe Cup (SPC), a Faraday cup pointing normal to the heat shield plane (Case  
 125 et al., 2020), two SPANe electron detectors (Whittlesey et al., 2020), one on either side  
 126 of the spacecraft but behind the heat shield, and one SPANi ion detector, also behind  
 127 the heat shield. The SPAN detectors are top hat electrostatic analyzers measuring the  
 128 distributions of electrons or protons from a few eV to  $\sim 30$  keV, at a cadence of  $\sim 13.98$   
 129 s for the second Venus encounter. SPC measures protons and alpha particle distributions  
 130 ( $\sim 100$  eV to  $\sim 8$  keV), primarily in the direction normal to the heat shield with a ca-  
 131 dence of  $\sim 0.87$  s. SPANi data are used as well when the flow deviates significantly from  
 132 the SPC field of view ( $\sim 13.98$  s cadence).

133 The Digital Fields Board (DFB) is a receiver within the FIELDS instrument (Malaspina  
 134 et al., 2016). DFB burst mode data are important to this study. These data consist of  
 135 six channels of data recorded at 150,000 samples per second (Sps) for intervals of  $\sim 3.5$ s.  
 136 During the second Venus encounter, these channels included differential voltages in the  
 137 heat shield plane ( $dV_{12} = V_1 - V_2, dV_{34} = V_3 - V_4$ ) and three orthogonal axes of SCM  
 138 data. The differential voltage data are band pass filtered, with -3 dB points near  $\sim 100$   
 139 Hz and  $\sim 60$  kHz. The SCM data band pass response has -3 dB points near  $\sim 20$  Hz and  
 140  $\sim 60$  kHz.

141 DFB high cadence data (150,000 Sps) are continuously recorded, then parsed into  
 142  $\sim 3.5$  s burst data intervals. Each burst data interval is assigned a quality flag, with a  
 143 value based on peak signal to noise ratio within a given burst interval. These intervals  
 144 enter a competitive queue. Intervals with the highest quality flags are kept, and others  
 145 discarded. The competitive queue stores 6 events at a time and events exit the queue  
 146 into the FIELDS on-board memory at the rate of one every  $\sim 20$  minutes. This time is  
 147 on the same order as the duration of the PSP Venus encounter. If a given event has high  
 148 signal to noise compared to subsequently recorded data, that event will persist in the  
 149 queue until it exits. Based on these considerations, FIELDS is expected to record  $\sim 6$   
 150 DFB burst data intervals within a few Venus radii of the planet, per Venus encounter.

### 151 3 Observations

152 Figure 1 presents an overview of the second PSP Venus encounter. Likely bow shock  
 153 crossings are indicated by vertical solid lines. A partial bow shock crossing near 18:06  
 154 UTC, suggests that PSP is skimming the bow shock.

155 Figure 1a shows the background magnetic field ( $\vec{B}$ ), including relatively steady and  
 156 weak fields in the solar wind at the start and end of the period, as well as enhanced mag-  
 157 nitude and fluctuations where the field piles up against Venus's induced magnetic field.  
 158 Figure 1b shows proton density (11 point median smoothed), with increases at the solar  
 159 wind / induced magnetosphere interface. Figure 1c shows proton bulk flow velocity  
 160 from SPC (11 point median smoothed), with clear slowing and deflection of solar wind  
 161 plasma. Figure 1d shows electron energy flux, with heating regions visible planet-ward  
 162 of each bow shock crossing. Figure 1e shows proton energy flux, with heating features  
 163 at each bow shock crossing. Figures 1f and 1g show on-board calculated power spectra  
 164 of differential voltage measurements in the heat shield plane for two frequency ranges.  
 165 Wave power is strongest and spans the most bandwidth at the bow shock crossings. The  
 166 magnetic field and particle data from these bow shock crossings are similar to those re-  
 167 ported previously (e.g. (Martinecz et al., 2009; Knudsen et al., 2016; Fränz et al., 2017))

168 Figures 1h and 1i show the geometry of the encounter in the x-y VSO plane. The  
 169 red curve shows a notional bow shock, modeled as a conic where  $r = L/(1 + \epsilon \cos(\theta))$ .  
 170 Values for the semilatus rectum  $L$ , the eccentricity  $\epsilon$ , and the conic focus  $x_0$  were cho-  
 171 sen by starting with typical values determined by (Martinez et al., 2009) and adjust-  
 172 ing them to minimize the distance between the shock surface and the first and last bow  
 173 shock crossings. The chosen values are  $L = 1.45 R_v$ ,  $\epsilon = 0.95$ ,  $x_0 = 0.64 R_v$ . The dot  
 174 dash lines shows the PSP trajectory from 17:58 to 18:26 UTC. In Figure 1h, black ar-  
 175 rows indicate the outward vector normal to the PSP heat shield. The heat shield plane  
 176 is indicated by green bars. Blue boxes indicate bow shock crossing times (vertical lines  
 177 in Figures 1a - 1d). In Figure 1i black crosses indicate DFB burst data times. Burst cap-  
 178 tures are triggered by high amplitude wave activity and cluster near bowshock crossings.

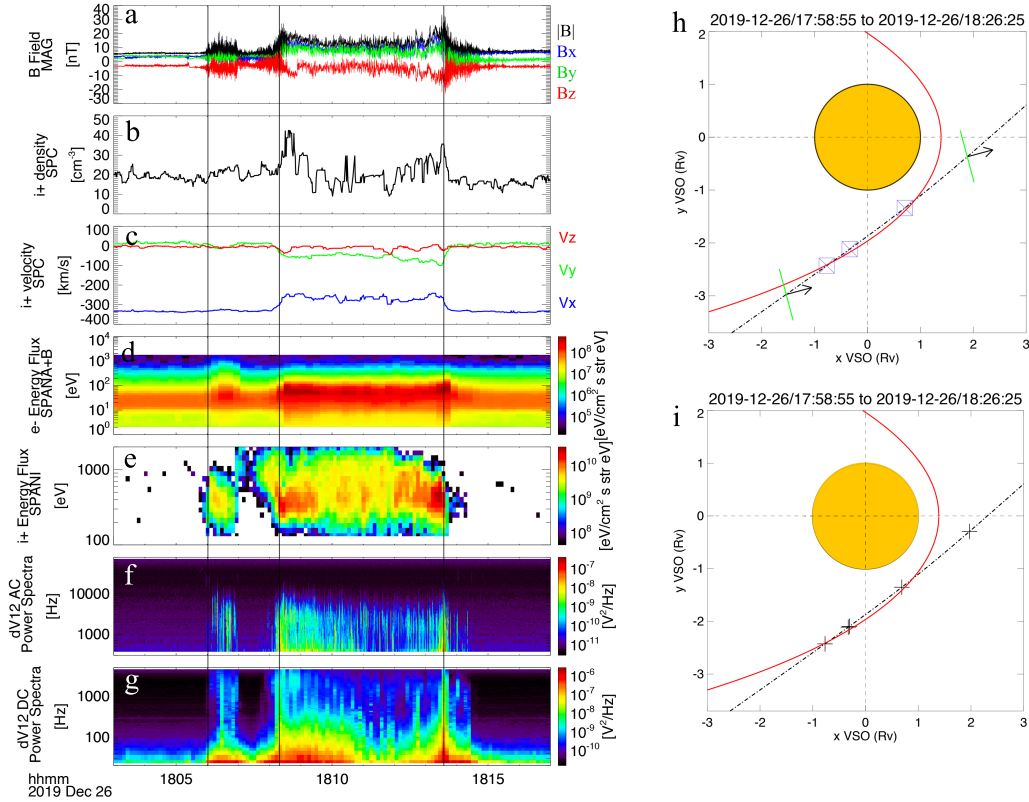


**Figure 1.** (a)  $|B|$  and  $\vec{B}$ , in VSO coordinates, (b) Proton density from SPC, (c) Proton flow velocity in VSO from SPC, (d) electron energy flux from SPANe, (e) proton energy flux from SPANi, (f) power spectra of  $V_1 - V_2$  differential voltages for  $\sim 400$  Hz to 75 kHz, (g) same as (f), but for  $\sim 20$  Hz to  $\sim 9.4$  kHz, (h) PSP trajectory (black dashed line) with notional bow shock (red line) and bow shock crossing times (blue boxes). A black arrow shows the outward normal to the heat shield. The green bar shows the heat shield plane. (i) Same as (h), with black crosses indicating burst data capture times.

179 Figure 2 shows plasma condition detail at inbound and outbound crossings of the  
 180 Venusian bow shock. Figures 2a,g show  $\vec{B}$  in VSO coordinates, with  $|B|$  plotted in black,  
 181 Figures 2b,h show proton energy flux from SPANi, Figures 2c,i show proton bulk flow  
 182 velocity in VSO from SPC (11 point median smoothed), Figures 2d,j show electron en-  
 183 ergy flux from SPANe, Figures 2e,k show electron core density determined by fits to the

184 core of the electron distribution as measured by SPANe (following the method of Halekas  
185 et al. (2020)). Figures 2f,l show electron core temperature determined by the same fits.

186 Vertical solid lines bracket burst data intervals, while vertical dashed lines indicate  
187 times when plasma double layers were observed (e.g. Figure 4). Burst data were recorded  
188 just planetward of each bow shock ramp, where  $|B|$  is enhanced by pile-up, the solar wind  
189 is slowed and deflected, and electrons are heated. Protons observed between  $\sim 18:07$  and  
190  $\sim 18:08$  UTC and after  $\sim 18:13$  UTC are likely reflected by interaction with the bow shock.  
191 Kinetic scale electric field structures, including double layers, are embedded in the re-  
192 gion where the strongest energy transfer from solar wind ram energy to particle heat-  
193 ing and flow deflection occurs.

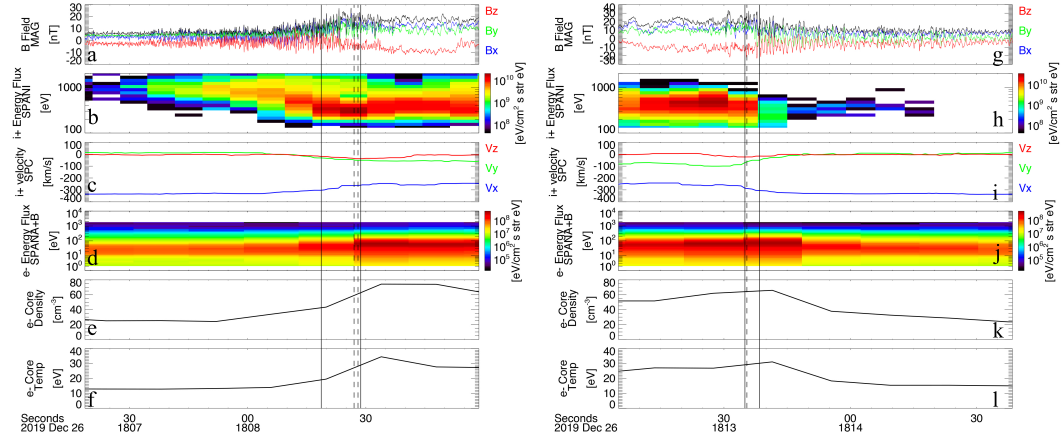


**Figure 2.** (a) Three components of  $\vec{B}$ , in VSO coordinates, (b) ion energy flux from SPANi, (c) Proton flow velocity in VSO from SPC, (d) electron energy flux from SPANe, (e,f) electron core density and temperature from fits to SPANe data. (g,h,i,j,k,l) Same quantities, for outbound bow shock crossing. Vertical solid line indicate start and stop times of FIELDS burst data, vertical lines indicate plasma double layer observations.

194 Figure 3 shows one burst interval dense with plasma double layers. Figure 3a shows  
195 differential voltage data from the two antenna pairs in the PSP heat shield plane, rotated  
196 into spacecraft body x-y coordinates. Figure 3b shows a windowed Fourier power spec-  
197 trum of the data in Figure 3a. Regions of intense high frequency electrostatic activity  
198 are indicated by vertical dashed lines and numbered. When these regions are examined  
199 in detail (see Figure 4), plasma double layers with developed two-stream electron insta-  
200 bilities are observed.

201 Several other electrostatic structures, including phase space holes and double lay-  
202 ers without developed instabilities, are also observed during this interval (see Figure 4).  
203 Data from the SCM are not shown because they contain only noise for this  $\sim 3.5$  s in-  
204 terval. The activity in Figure 3 is electrostatic to the sensitivity of the SCM as operated  
205 during this encounter.

206 Figures 4a - 4p show waveforms for four double layers with developed streaming  
207 instabilities, numbered corresponding to Figure 3. Each double layer is described by four  
208 panels, each showing two orthogonal differential voltage signals in the heat shield plane,  
209 rotated into a maximum variance coordinate system. The maximum variance direction  
210 is determined using the narrow interval around each double layer (gray shading). Each  
211 panel shows the maximum variance (top) and perpendicular components (bottom). Fig-  
212 ures 4a,e,i,m show an extended monopolar electric field bounding a region of rapidly os-

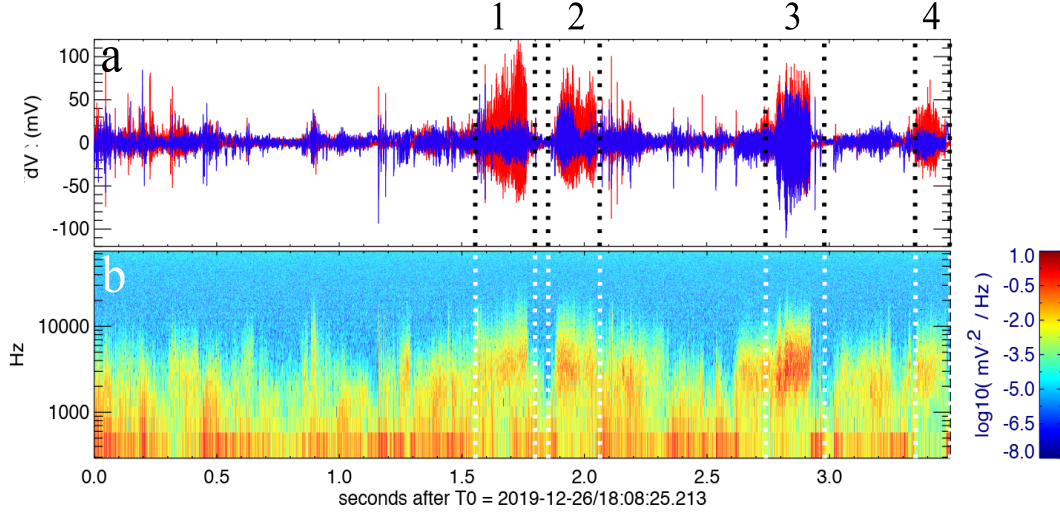


**Figure 3.** (a) Time series differential voltage waveforms in the heat shield plane, in spacecraft body coordinates. The blue trace indicates spacecraft x (close to the ecliptic plane), the red trace spacecraft y (close to normal to the ecliptic). Vertical lines indicate intervals with plasma double layers. (b) Windowed Fourier transform of the data in (a).

213 cillating electric field. Figures 4b,f,j,n and 4c,g,k,o and 4d,h,l,p show electric fields from  
 214 regions at times indicated by the vertical red lines. In each case, three red vertical lines  
 215 correspond to the three sets of small plots showing early, middle, and late times in each  
 216 double layer example. For example, Figure 4f corresponds to the time indicated by the  
 217 left-most red line in Figure 4e. In each case, electric field fluctuations are least structured  
 218 close to the double layer and progressively evolve into coherent bipolar structures (most  
 219 evident in Figure 4b and Figure 4h). Figures 4q and 4r are described below.

220 These observations are consistent with simulated (e.g. (Newman et al., 2001; Gold-  
 221 man et al., 2008)) and observed (e.g. (Andersson et al., 2002; Ergun et al., 2009; Malaspina  
 222 et al., 2014)) doubler-layer driven two-stream instability, where coherent phase space vor-  
 223 tices, recognizable as bipolar electric field pulses (e.g. Figure 4b), form some distance  
 224 from the double layer.

225 Additionally, this interval contains  $\sim 10$  monopolar electric field pulses without de-  
 226 veloped streaming instability signatures (e.g. Figure 4i, far right). These pulses have their  
 227 largest amplitude in the maximum variance coordinate system defined by the identified  
 228 double layers, consistent with the interpretation that they are also double layers.

229 The spatial scale and potential drop associated with each double layer in Figure  
 230 4 can be estimated. To do so, it is assumed (following (Ergun et al., 2009)) that the dou-  
 231 ble layers propagate parallel or anti-parallel to the background magnetic field direction  
 232 ( $\hat{B}$ ) at the ion sound speed ( $c_s$ ). The effective velocity of the double layer in the frame  
 233 of the spacecraft ( $v_{eff}$ ) is therefore  $\vec{v}_{eff} = (\pm c_s \hat{B}) + \vec{v}_{sc} + \vec{v}_p$ , where  $\vec{v}_{sc}$  is the space-  
 234 craft velocity and  $\vec{v}_p$  is the proton bulk flow velocity. Here, all velocities are in VSO co-  
 235 ordinates. Because each of these velocities ( $c_s, v_{sc}, v_p$ ) are of similar magnitude, it is likely  
 236 that the spacecraft encounters the double layer at an oblique angle. Figure 4r shows this  
 237 geometry in the plane defined by  $\hat{B}$  and  $\vec{v}_{eff}$ . The double layer width is then  $L_{DL} =$   
 238  $|v_{eff}| dt_{DL} \sin(\psi)$ .  $\psi$  is defined as  $\theta_{B,v_{eff}} - 90^\circ$ , where  $\theta_{B,v_{eff}}$  is the angle between  
 239 the background magnetic field direction and the effective velocity vector. Because it is



240 not known a-priori whether the double layer is propagating along  $\hat{B}$  or  $-\hat{B}$ , two  $L_{DL}$  results are possible for each double layer.  
241

242 For double layers 1-4 in Figure 4, estimated  $L_{DL}$  are  $37\lambda_D$ ,  $62\lambda_D$ ,  $71\lambda_D$ ,  $155\lambda_D$ ,  
243 respectively, for Debye length  $\lambda_D$ . Here,  $\bar{v}_p$  and the proton temperature are defined using  
244 the SPC sample closest in time to each double layer. SPANi proton core distribution  
245 fitting indicates a maximum flow deviation of  $\sim 13^\circ$  from the spacecraft z axis, and  
246 SPC data are valid for flows  $\pm 30^\circ$  from spacecraft z (Kasper et al., 2016), therefore we  
247 use SPC data for ion properties. Electron core density and temperature are derived from  
248 fits to SPANe data (following (Halekas et al., 2020)).

249 The estimated spatial scales (few tens of Debye lengths) are consistent with prior  
250 studies at Earth (e.g. (Ergun et al., 2009) and references therein), except for the 4th double  
251 layer, which is a factor of 2 or 3 larger than expected. Figure 4q shows  $\hat{B}$  (blue) and  
252  $\hat{v}_{eff}$  for propagation along  $\hat{B}$  (purple solid) and  $-\hat{B}$  (purple dashed), with respect to the  
253 heat shield plane (green), with all vectors projected into the x-y VSO plane. Reasonable  
254 values for  $L_{DL}$  require propagation along  $\hat{B}$  (generally away from Venus). Assuming prop-  
255 agation along  $-\hat{B}$  results in  $L_{DL} \gg 500 \lambda_D$ , which is too large to maintain charge sep-  
256 aration.

257 Each double layer's potential drop can be estimated as  $\Phi = \int E_{\parallel} dl$ , where  $\int E_{\parallel} dl =$   
258  $(\int E_{\parallel} dt) \cdot (|v_{eff}| \sin(\psi))$  where  $dt$  is the inverse sample rate. Only the projection of  $E_{\parallel}$   
259 in the heat shield plane can be measured accurately, but  $E_{\parallel}$  can be estimated as  $E_{measured}/\cos(\theta_{Bxy})$ ,  
260 where  $\theta_{Bxy}$  is the angle between  $\vec{B}$  and the heat shield plane (x-y plane in spacecraft co-  
261 ordinates). A further complication is that the effective electrical length of the antenna  
262 is unknown at these frequencies at this time. Therefore it is useful to define,  $E_{measured} =$   
263  $-dV_{measured}/L_{eff}$  for the differential voltage measurements ( $dV$ ) shown in Figure 4. As-  
264 suming  $L_{eff} \approx 1\text{m}$ , and integrating over the grey regions marked for the four double  
265 layers, the potential drops are estimated to be  $\Phi = 13\text{ V}$ ,  $9\text{ V}$ ,  $32\text{ V}$ , and  $86\text{ V}$ . A longer  
266 effective electrical length linearly reduces the potential drop estimates. Given the ap-  
267 proximations used, additional precision on the voltage drop estimates is not meaning-  
268 ful.

269 These potential drops, except possibly the 4th, are similar to the electron temper-  
270 ature gradient across the bow shock (Figure 2), leaving open the possibility that these  
271 double layers are either (i) formed as hot sheath electrons mix with cold solar wind elec-  
272 trons, or (ii) accelerating solar wind electrons to a significant fraction of the sheath tem-  
273 perature as they encounter the double layer electric potential. Future studies are required  
274 to evaluate these scenarios. The first possibility is consistent with simulations of double  
275 layers separating hot and cold electron populations, which have found that double  
276 layer potential drops can be limited by the hot electron temperature (T. C. Li et al., 2013).

## 277 4 Discussion

278 The plasma double layers and associated kinetic scale electric field structures are  
279 observed just planetward of the bow shock magnetic ramp, a narrow spatial region where  
280 solar wind particles are undergo deceleration, deflection and heating. A study by (Knudsen  
281 et al., 2016) explored this region with data from Pioneer Venus, inferring that "...non-  
282 Maxwellian ... electron velocity distributions colocated with the magnetic field ramp oc-  
283 cur in a continuous but convoluted layer of the order of 100 to 200 km thick." The cur-  
284 rent observations of kinetic plasma structures within the shock ramp are entirely con-  
285 sistent with this, and double layers naturally explain the presence of non-Maxwellian elec-  
286 tron velocity distributions.

287 FIELDS returned five  $\sim 3.5\text{s}$  DFB burst captures during the  $\sim 15$  minute 2nd Venus  
288 encounter. Four were recorded as the spacecraft skimmed the bow shock, and two con-  
289 tained signatures of plasma double layers. Even with this limited data set, at least six

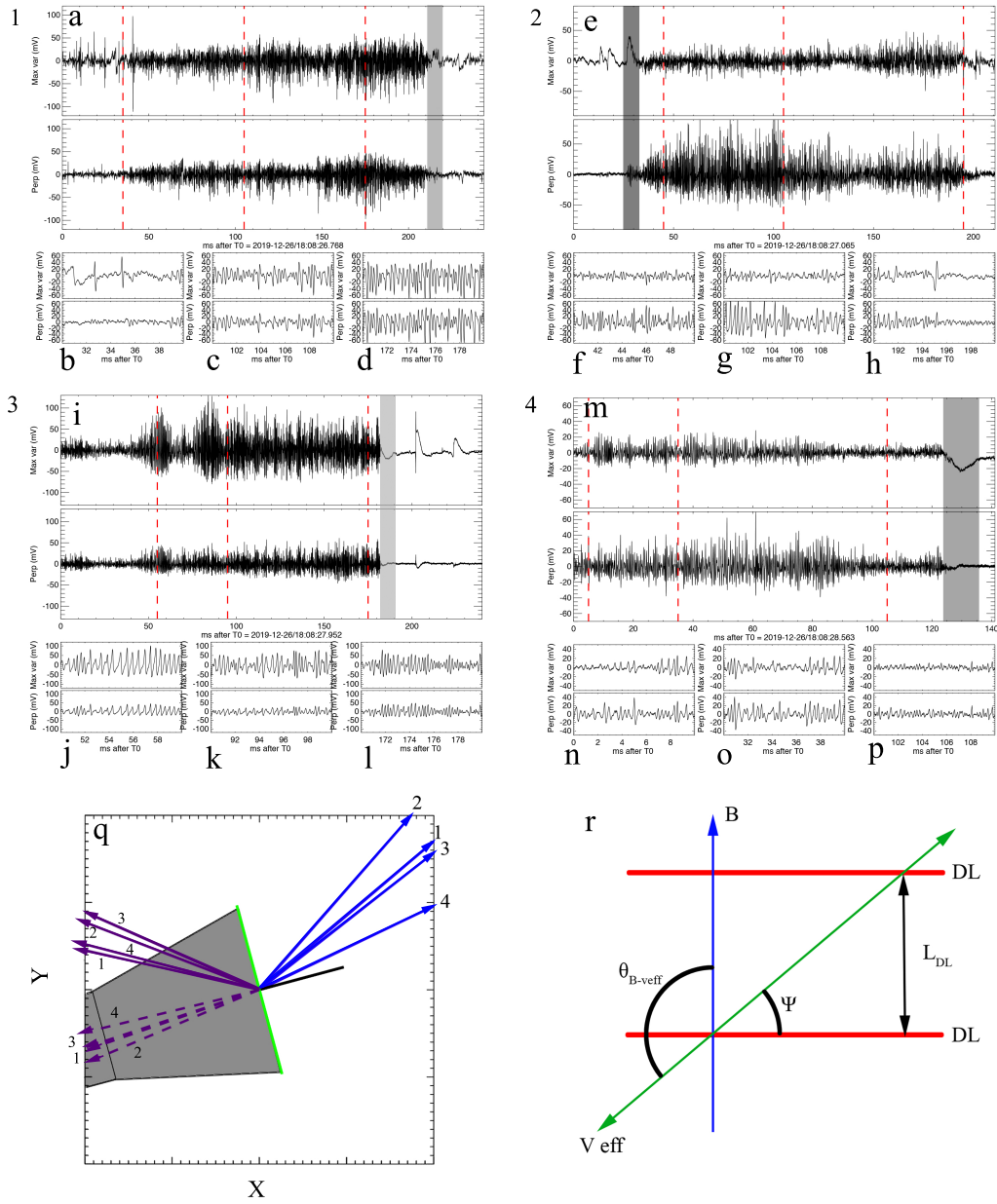


**Figure 4.** Each pair of panels shows time domain differential voltage data along two directions in the plane of the heat shield: maximum variance (top) and perpendicular (bottom). (a) shows a double layer (gray shading) with attendant electrostatic waves. (b,c,d) show data from sub-intervals of (a) at times indicated by vertical red lines. (e,f,g,h), (i,j,k,l), (m,n,o,p), have the same format as (a,b,c,d), but for three other double layers. (q) Vectors, for each of the four double layers, projected into the x-y VSO plane, for the magnetic field (blue), effective double layer velocity assuming  $\vec{v}_{eff} \parallel \vec{B}$  (solid purple) and assuming  $\vec{v}_{eff} \parallel -\vec{B}$  (dashed purple). The heat shield plane is shown in green, and its normal vector in black. A cartoon spacecraft bus is shown in gray. (r) Geometry of an oblique double layer crossing, in a plane containing  $\vec{B}$  (blue) and  $\vec{v}_{eff}$  (green).



290 double layers with active streaming instabilities (four shown here), and at least ten likely  
291 double layers without streaming instabilities, were observed. By comparison, decades of  
292 burst captures by missions traversing Earth's bow shock (Geotail, Cluster, THEMIS, MMS)  
293 yielded two published observations of double layers (S. Li et al., 2015; Goodrich et al.,  
294 2018). (S. Li et al., 2015) identified 9 distinct double layers in one shock crossing. (Goodrich  
295 et al., 2018) identified one double layer in one shock crossing.

296 One possible explanation relates to how plasma waves at Earth and Venus inter-  
297 act with burst data capture systems. Fields data burst capture systems are generally  
298 configured to trigger on the largest amplitude signals in a given interval. This is true for  
299 both near-Earth missions and PSP at Venus. Near Earth's bow shock, there are many  
300 high amplitude, high frequency waves (e.g. (Wilson et al., 2014) and references therein)  
301 to trigger burst captures. Structures like double layers are lower amplitude and there-  
302 fore are less likely to trigger a capture. If, at Venus, double layers and the electrostatic  
303 waves they drive have amplitudes higher than other shock- and sheath-driven high fre-  
304 quency waves (consistent with Figure 1f and Figure 1g), they would be preferentially se-  
305 lected by the burst trigger algorithm.

306 The estimated spatial scales and potential drops are consistent with prior studies  
307 (e.g. (Ergun et al., 2009) and references therein) for three of the four double layers in-  
308 vestigated. Estimates for the fourth are too large and too deep, possibly due to the steep  
309 angle of  $\hat{B}$  with respect to the heat shield (Figure 4q), for which measurements in the  
310 heat shield plane are less representative of the parallel electric field, or possibly due to  
311 under-estimate of effective electrical length.

## 312 5 Conclusions

313 This work reports the first observation of a plasma double layer outside of near-  
314 Earth space, and the first observations of kinetic-scale electric field structures at Venus's  
315 induced magnetosphere. The morphology of the time-series data, estimated spatial scales,  
316 and estimated potential depths are all consistent with observations of double layers ob-  
317 served in Earth's magnetosphere. These structures are observed on the planetward side  
318 of the bow shock magnetic ramp, where solar wind particles are being slowed, deflected,  
319 and heated. Their presence demonstrates that kinetic plasma physics processes are ac-  
320 tive in the slowing, deflection, and heating of solar wind particles at the Venus induced  
321 magnetosphere. Observations of these structures on future PSP Venus encounters or by  
322 a future Venus space plasma investigation may help determine whether double layers at  
323 the Venus bow shock are driven by field aligned currents in the draped IMF magnetic  
324 field lines, or by the mixing of solar wind and magnetosheath plasma. Finally, the ob-  
325 servations reported here imply that kinetic scale plasma phenomena, and in particular  
326 structures with parallel electric fields, are likely active in plasma environments with sig-  
327 nificant wave-particle energy transfer, even if they have not yet been observed.

## 328 Acknowledgments

329 The authors thank the Parker Solar Probe, FIELDS and SWEAP teams. The FIELDS  
330 experiment on Parker Solar Probe was designed and developed under NASA contract  
331 NNN06AA01C. TD acknowledges support from CNES. All data used here are available  
332 on the FIELDS and SWEAP data archives:  
333 <http://fields.ssl.berkeley.edu/data/>, <http://sweap.cfa.harvard.edu/pub/data/sci/sweap/>

## 334 References

335 Andersson, L., Ergun, R. E., Newman, D. L., McFadden, J. P., Carlson, C. W.,  
336 & Su, Y.-J. (2002, August). Characteristics of parallel electric fields in the  
337 downward current region of the aurora. *Physics of Plasmas*, *9*, 3600-3609. doi:

- 338 10.1063/1.1490134
- 339 Bale, S. D., Goetz, K., Harvey, P. R., Turin, P., Bonnell, J. W., Dudok de Wit, T.,  
340 ... Wygant, J. R. (2016, December). The FIELDS Instrument Suite for Solar  
341 Probe Plus. Measuring the Coronal Plasma and Magnetic Field, Plasma Waves  
342 and Turbulence, and Radio Signatures of Solar Transients. *Space Science*  
343 *Reviews*, 204(1-4), 49-82. doi: 10.1007/s11214-016-0244-5
- 344 Case, A. W., Kasper, J. C., Stevens, M. L., Korreck, K. E., Paulson, K., Daigneau,  
345 P., ... Martinović, M. M. (2020, February). The Solar Probe Cup on the  
346 Parker Solar Probe. *The Astrophysical Journal Supplement*, 246(2), 43. doi:  
347 10.3847/1538-4365/ab5a7b
- 348 Cattell, C., Crumley, J., Dombeck, J., Wygant, J. R., & Mozer, F. S. (2002, March).  
349 Polar observations of solitary waves at the Earth's magnetopause. *Geophysical*  
350 *Review Letters*, 29, 1065. doi: 10.1029/2001GL014046
- 351 Ergun, R. E., Andersson, L., Tao, J., Angelopoulos, V., Bonnell, J., McFadden,  
352 J. P., ... Baumjohann, W. (2009, April). Observations of Double Layers  
353 in Earth's Plasma Sheet. *Physical Review Letters*, 102(15), 155002. doi:  
354 10.1103/PhysRevLett.102.155002
- 355 Ergun, R. E., Su, Y.-J., Andersson, L., Carlson, C. W., McFadden, J. P., Mozer,  
356 F. S., ... Strangeway, R. J. (2001, July). Direct Observation of Localized Par-  
357 allel Electric Fields in a Space Plasma. *Physical Review Letters*, 87(4), 045003.  
358 doi: 10.1103/PhysRevLett.87.045003
- 359 Fox, N. J., Velli, M. C., Bale, S. D., Decker, R., Driesman, A., Howard, R. A.,  
360 ... Lario, D. (2016, Dec). The Solar Probe Plus Mission: Humanity's  
361 First Visit to Our Star. *Space Science Reviews*, 204(1-4), 7-48. doi:  
362 10.1007/s11214-015-0211-6
- 363 Franz, J. R., Kintner, P. M., & Pickett, J. S. (1998). POLAR observations of coher-  
364 ent electric field structures. *Geophysical Research Letters*, 25, 1277-1280. doi:  
365 10.1029/98GL50870
- 366 Fränz, M., Echer, E., Marques de Souza, A., Dubinin, E., & Zhang, T. L. (2017,  
367 October). Ultra low frequency waves at Venus: Observations by the  
368 Venus Express spacecraft. *Planetary and Space Sciences*, 146, 55-65. doi:  
369 10.1016/j.pss.2017.08.011
- 370 Fu, H. S., Chen, F., Chen, Z. Z., Xu, Y., Wang, Z., Liu, Y. Y., ... Burch, J. L.  
371 (2020, Mar). First measurements of electrons and waves inside an elec-  
372 trostatic solitary wave. *Phys. Rev. Lett.*, 124, 095101. Retrieved from  
373 <https://link.aps.org/doi/10.1103/PhysRevLett.124.095101> doi:  
374 10.1103/PhysRevLett.124.095101
- 375 Futaana, Y., Stenberg Wieser, G., Barabash, S., & Luhmann, J. G. (2017, Novem-  
376 ber). Solar Wind Interaction and Impact on the Venus Atmosphere. *Space*  
377 *Science Reviews*, 212(3-4), 1453-1509. doi: 10.1007/s11214-017-0362-8
- 378 Goldman, M. V., Newman, D. L., & Pritchett, P. (2008, November). Vlasov sim-  
379 ulations of electron holes driven by particle distributions from PIC recon-  
380 nection simulations with a guide field. *Geophys. Res. Lett.*, 35, 22109. doi:  
381 10.1029/2008GL035608
- 382 Goodrich, K. A., Ergun, R., Schwartz, S. J., Wilson, L. B., Newman, D., Wilder,  
383 F. D., ... Andersson, L. (2018, November). MMS Observations of Electro-  
384 static Waves in an Oblique Shock Crossing. *Journal of Geophysical Research*  
385 *(Space Physics)*, 123(11), 9430-9442. doi: 10.1029/2018JA025830
- 386 Gurnett, D. A., Zarka, P., Manning, R., Kurth, W. S., Hospodarsky, G. B.,  
387 Averkamp, T. F., ... Farrell, W. M. (2001, January). Non-detection at Venus  
388 of high-frequency radio signals characteristic of terrestrial lightning. *Nature*,  
389 409(6818), 313-315.
- 390 Halekas, J. S., Whittlesey, P., Larson, D. E., McGinnis, D., Maksimovic, M.,  
391 Berthomier, M., ... Harvey, P. R. (2020, February). Electrons in the Young  
392 Solar Wind: First Results from the Parker Solar Probe. *The Astrophysical*

- 393 Journal Supplement, 246(2), 22. doi: 10.3847/1538-4365/ab4cec
- 394 Holmes, J. C., Ergun, R. E., Newman, D. L., Ahmadi, N., Andersson, L., Le Con-  
395 tel, O., . . . Burch, J. L. (2018, December). Electron Phase-Space Holes in  
396 Three Dimensions: Multispacecraft Observations by Magnetospheric Multi-  
397 scale. Journal of Geophysical Research (Space Physics), 123, 9963-9978. doi:  
398 10.1029/2018JA025750
- 399 Holmes, J. C., Ergun, R. E., Newman, D. L., Wilder, F. D., Sturmer, A. P.,  
400 Goodrich, K. A., . . . Burch, J. L. (2018, January). Negative Potent-  
401 tial Solitary Structures in the Magnetosheath With Large Parallel Width.  
402 Journal of Geophysical Research (Space Physics), 123(1), 132-145. doi:  
403 10.1002/2017JA024890
- 404 Hutchinson, I. H. (2017, may). Electron holes in phase space: What they are and  
405 why they matter. Physics of Plasmas, 24(5), 055601. Retrieved from [http://](http://aip.scitation.org/doi/10.1063/1.4976854)  
406 [aip.scitation.org/doi/10.1063/1.4976854](http://aip.scitation.org/doi/10.1063/1.4976854) doi: 10.1063/1.4976854
- 407 Kasper, J. C., Abiad, R., Austin, G., Balat-Pichelin, M., Bale, S. D., Belcher, J. W.,  
408 . . . Zank, G. (2016, December). Solar Wind Electrons Alphas and Protons  
409 (SWEAP) Investigation: Design of the Solar Wind and Coronal Plasma Instru-  
410 ment Suite for Solar Probe Plus. Space Science Reviews, 204(1-4), 131-186.  
411 doi: 10.1007/s11214-015-0206-3
- 412 Klimov, S., Savin, S., Sokolov, A., Oberc, P., Orlowski, D., & Woźniak, D. (1986,  
413 January). First results of the VEGA low-frequency plasma wave analyser  
414 APV-N. In Field, particle and wave experiments on cometary missions (p. 169-  
415 174).
- 416 Knudsen, W. C., Jones, D. E., Peterson, B. G., & Knadler, C. E. (2016, August).  
417 Measurement of solar wind electron density and temperature in the shocked  
418 region of Venus and the density and temperature of photoelectrons within the  
419 ionosphere of Venus. Journal of Geophysical Research (Space Physics), 121(8),  
420 7753-7770. doi: 10.1002/2016JA022526
- 421 Li, S., Zhang, S., Cai, H., Bai, X., & Xie, Q. (2015, April). Characteristics of the  
422 double layer associated with terrestrial bow shock by THEMIS observation.  
423 Science China Earth Sciences, 58(4), 562-572. doi: 10.1007/s11430-014-5040-z
- 424 Li, T. C., Drake, J. F., & Swisdak, M. (2013, December). Coronal Electron Confinement  
425 by Double Layers. The Astrophysical Journal, 778(2), 144. doi: 10.1088/  
426 0004-637X/778/2/144
- 427 Malaspina, D. M., Andersson, L., Ergun, R. E., Wygant, J. R., Bonnell, J. W., Klet-  
428 zing, C., . . . Larsen, B. A. (2014, August). Nonlinear electric field structures  
429 in the inner magnetosphere. Geophysical Review Letters, 41, 5693-5701. doi:  
430 10.1002/2014GL061109
- 431 Malaspina, D. M., Ergun, R. E., Bolton, M., Kien, M., Summers, D., Stevens, K., . . .  
432 Bale, S. D. (2016, Jun). The Digital Fields Board for the FIELDS instrument  
433 suite on the Solar Probe Plus mission: Analog and digital signal processing.  
434 Journal of Geophysical Research (Space Physics), 121(6), 5088-5096. doi:  
435 10.1002/2016JA022344
- 436 Martinecz, C., Boesswetter, A., FränZ, M., Roussos, E., Woch, J., Krupp, N., . . .  
437 Kulikov, Y. (2009, September). Plasma environment of Venus: Compar-  
438 ison of Venus Express ASPERA-4 measurements with 3-D hybrid simula-  
439 tions. Journal of Geophysical Research (Planets), 114(E9), E00B30. doi:  
440 10.1029/2008JE003174
- 441 Martinecz, C., FränZ, M., Woch, J., Krupp, N., Roussos, E., Dubinin, E., . . . Lam-  
442 mer, H. (2008, May). Location of the bow shock and ion composition  
443 boundaries at Venus—initial determinations from Venus Express ASPERA-4.  
444 Planetary and Space Sciences, 56(6), 780-784. doi: 10.1016/j.pss.2007.07.007
- 445 Matsumoto, H., Kojima, H., Miyatake, T., Omura, Y., Okada, M., Nagano, I., &  
446 Tsutsui, M. (1994, December). Electrotastic Solitary Waves (ESW) in the  
447 magnetotail: BEN wave forms observed by GEOTAIL. Geophysical Research

- 448 Letters, 21, 2915-2918. doi: 10.1029/94GL01284
- 449 Mozer, F. S., Agapitov, O., Krasnoselskikh, V., Lejosne, S., Reeves, G. D., & Roth,  
450 I. (2014, July). Direct Observation of Radiation-Belt Electron Acceleration  
451 from Electron-Volt Energies to Megavolts by Nonlinear Whistlers. Physical  
452 Review Letters, 113(3), 035001. doi: 10.1103/PhysRevLett.113.035001
- 453 Mozer, F. S., Bale, S. D., Bonnell, J. W., Chaston, C. C., Roth, I., & Wygant,  
454 J. (2013, December). Megavolt Parallel Potentials Arising from Double-  
455 Layer Streams in the Earth's Outer Radiation Belt. Physical Review Letters,  
456 111(23), 235002. doi: 10.1103/PhysRevLett.111.235002
- 457 Newman, D. L., Goldman, M. V., Ergun, R. E., & Mangeney, A. (2001, De-  
458 cember). Formation of Double Layers and Electron Holes in a Current-  
459 Driven Space Plasma. Physical Review Letters, 87(25), 255001. doi:  
460 10.1103/PhysRevLett.87.255001
- 461 Pickett, J., Chen, L., Kahler, S., Santolík, O., Gurnett, D., Tsurutani, B., & Balogh,  
462 A. (2004, July). Isolated electrostatic structures observed throughout the  
463 Cluster orbit: relationship to magnetic field strength. Annales Geophysicae,  
464 22, 2515-2523. doi: 10.5194/angeo-22-2515-2004
- 465 Pickett, J. S., Menietti, J. D., Gurnett, D. A., Tsurutani, B., Kintner, P. M., Klatt,  
466 E., & Balogh, A. (2003). Solitary potential structures observed in the mag-  
467 netosheath by the Cluster spacecraft. Nonlinear Processes in Geophysics, 10,  
468 3-11.
- 469 Russell, C. T., Luhmann, J. G., & Strangeway, R. J. (2006, November). The  
470 solar wind interaction with Venus through the eyes of the Pioneer Venus  
471 Orbiter. Planetary and Space Sciences, 54(13-14), 1482-1495. doi:  
472 10.1016/j.pss.2006.04.025
- 473 Schamel, H. (2012, February). Cnoidal electron hole propagation: Trapping, the for-  
474 gotten nonlinearity in plasma and fluid dynamics. Physics of Plasmas, 19(2),  
475 020501. doi: 10.1063/1.3682047
- 476 Whittlesey, P. L., Larson, D. E., Kasper, J. C., Halekas, J., Abatcha, M., Abiad, R.,  
477 ... Verniero, J. L. (2020, February). The Solar Probe ANalyzers—Electrons  
478 on the Parker Solar Probe. The Astrophysical Journal Supplement, 246(2), 74.  
479 doi: 10.3847/1538-4365/ab7370
- 480 Wilson, L. B., Sibeck, D. G., Breneman, A. W., Le Contel, O., Cully, C., Turner,  
481 D. L., ... Malaspina, D. M. (2014, August). Quantified energy dis-  
482 sipation rates in the terrestrial bow shock: 2. Waves and dissipation.  
483 Journal of Geophysical Research (Space Physics), 119(8), 6475-6495. doi:  
484 10.1002/2014JA019930

Figure 1.

Author Manuscript



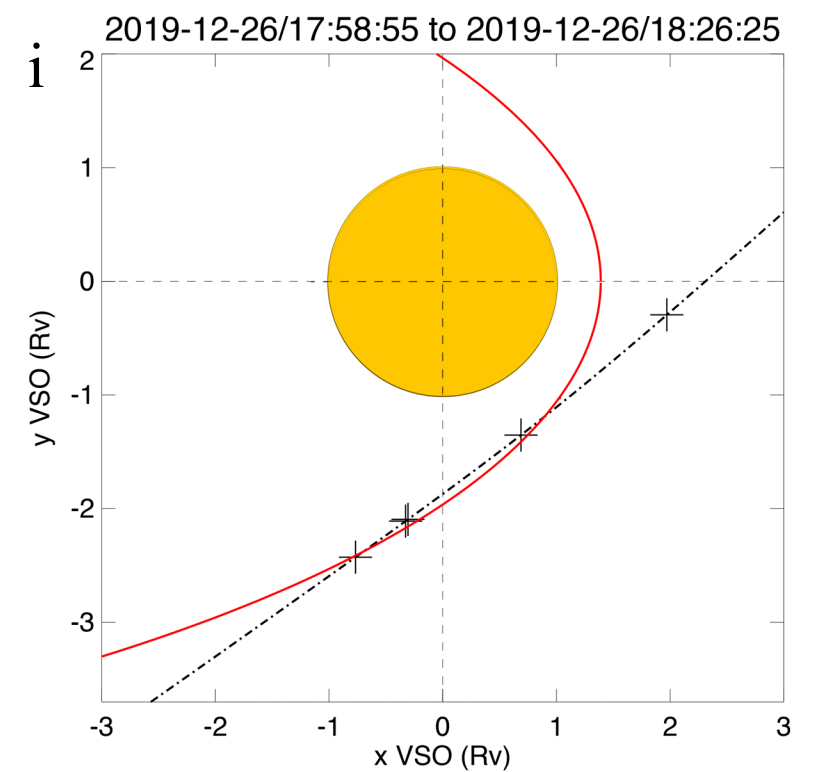
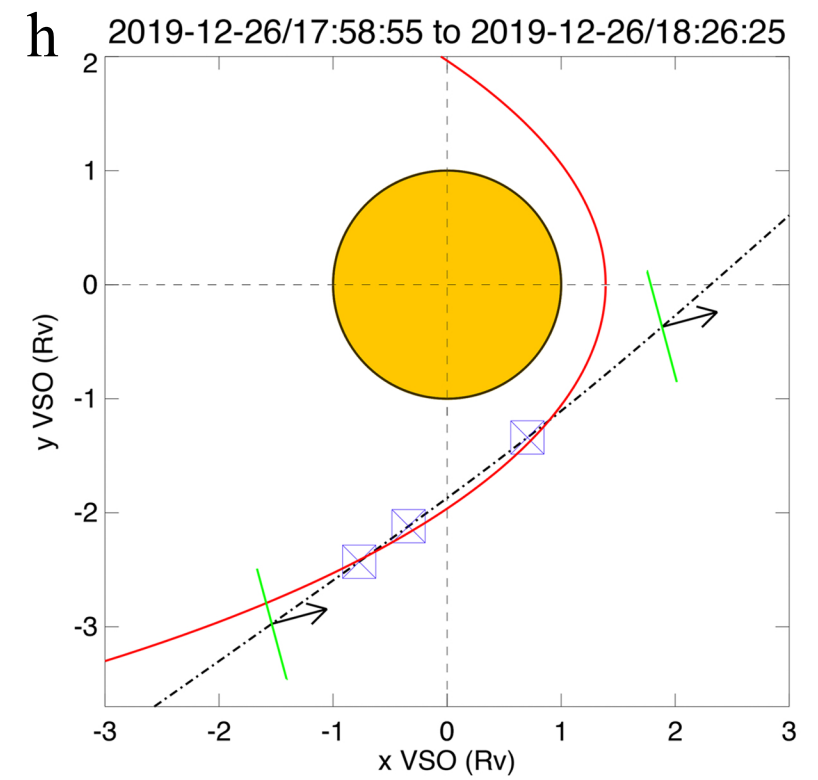
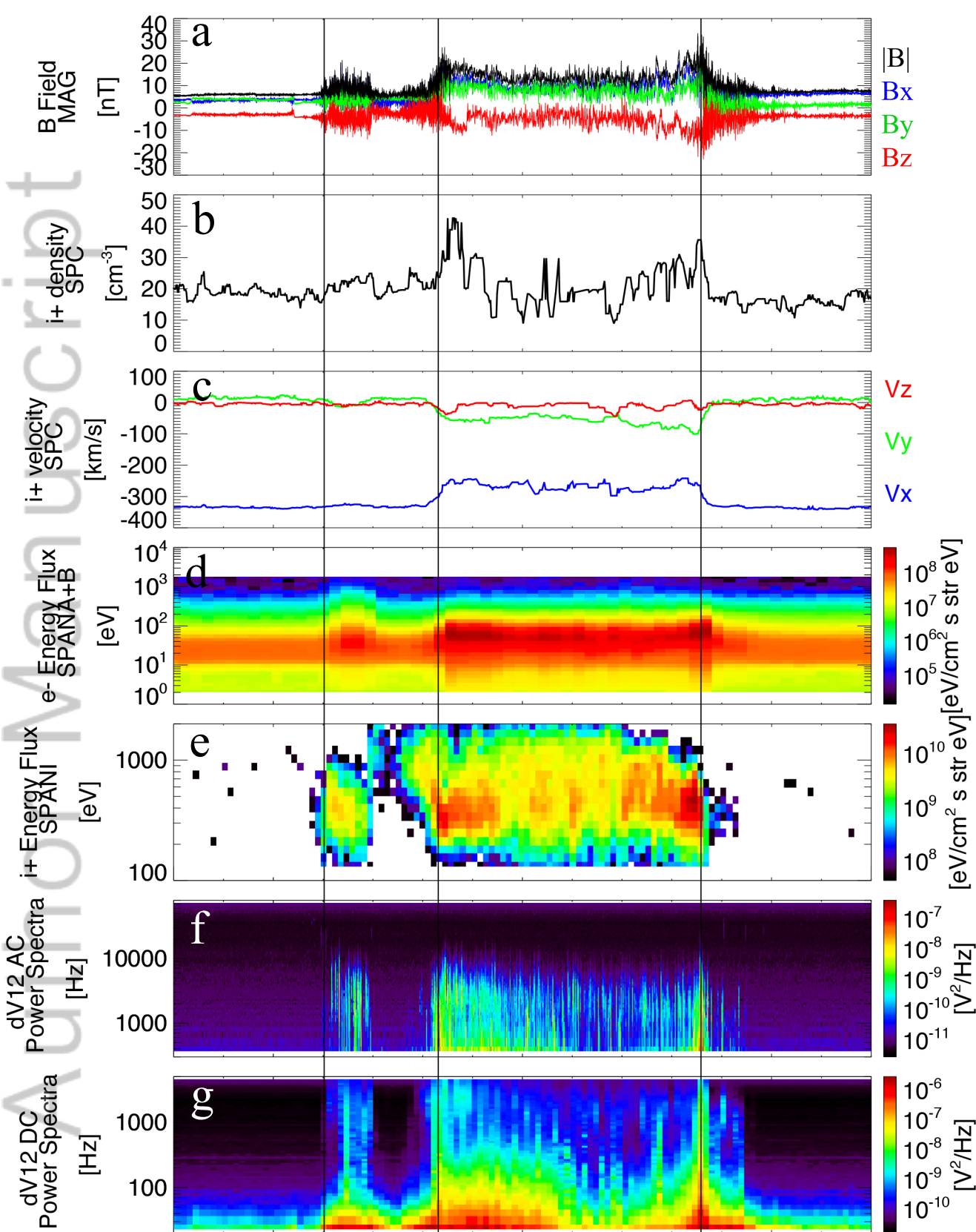


Figure 2.

Author Manuscript



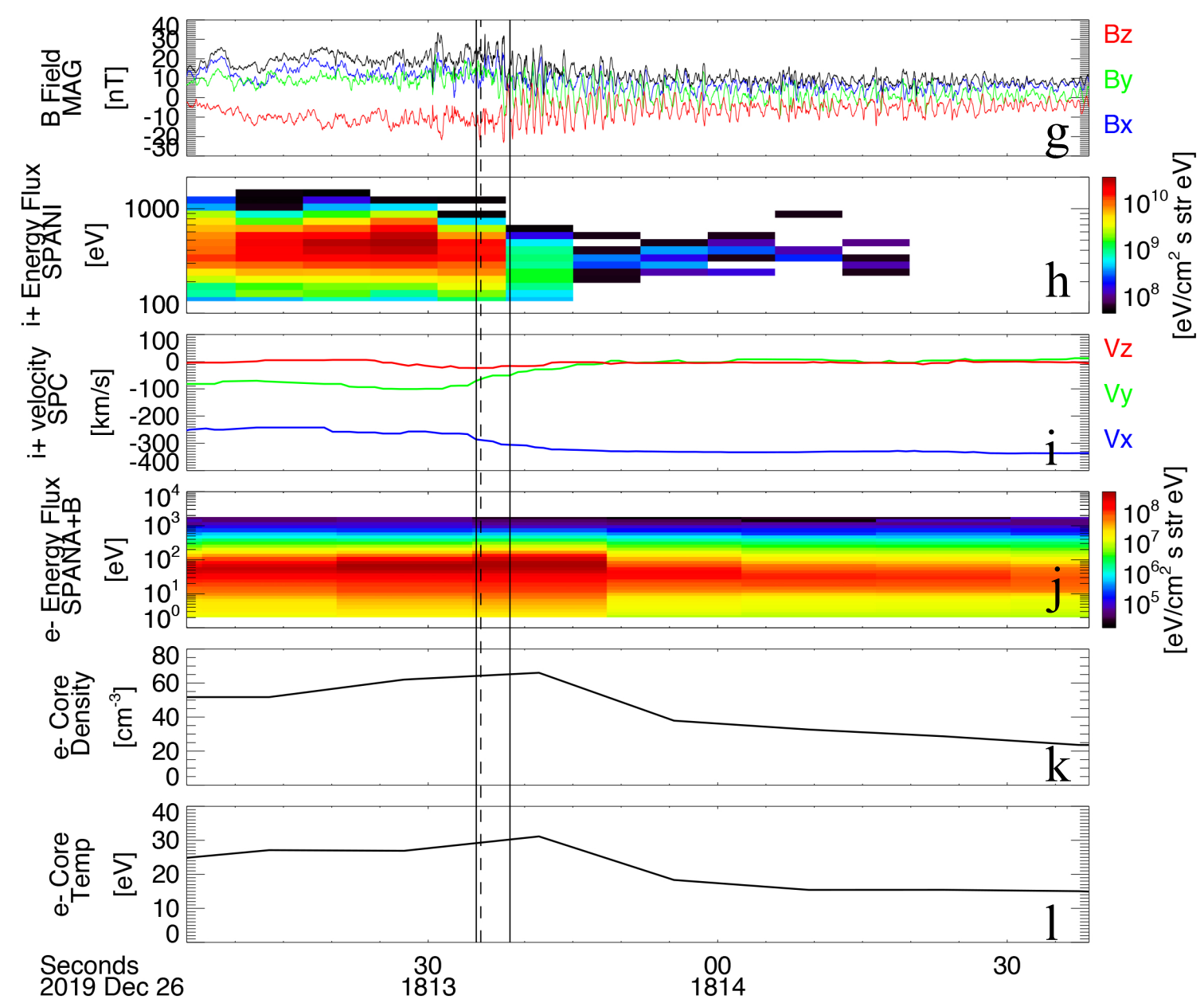
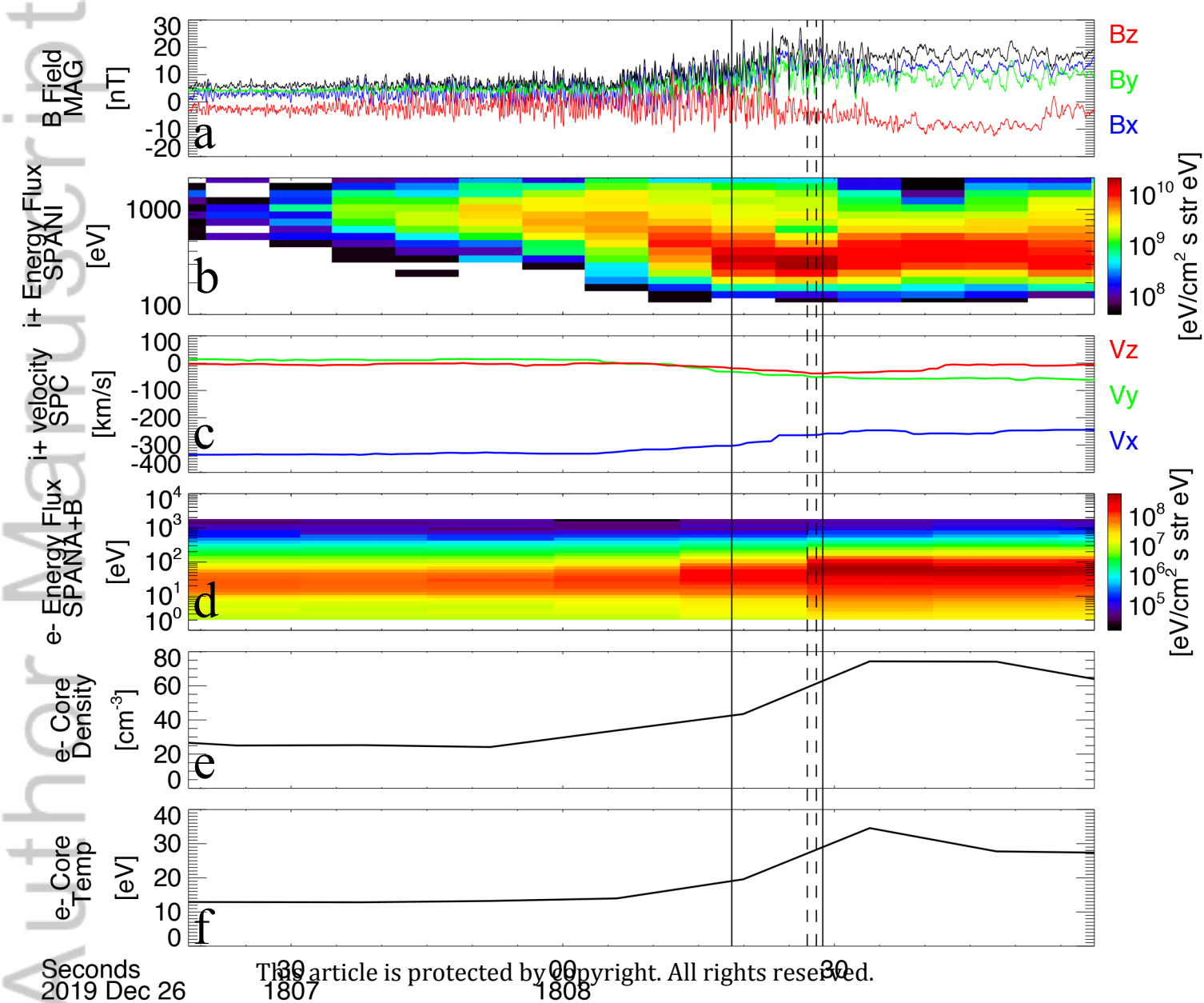


Figure 3.

Author Manuscript

1 2 3 4

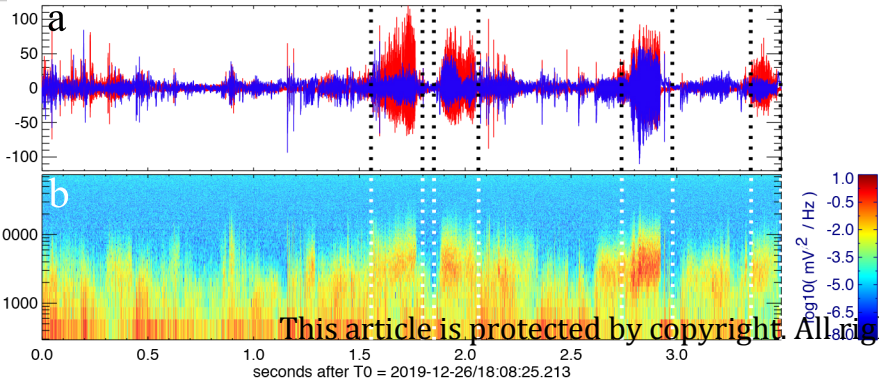


Figure 4.

Author Manuscript

